Research article

JHEP|Reports

Biliary atresia susceptibility gene EFEMP1 regulates extrahepatic bile duct elastic fiber formation and mechanics

Authors

Kapish Gupta, Jessica Llewellyn, Emilia Roberts, …, Ali Naji, Richard K. Assoian, Rebecca G. Wells

Correspondence

rgwells@pennmedicine.upenn.edu (R.G. Wells).

Graphical abstract

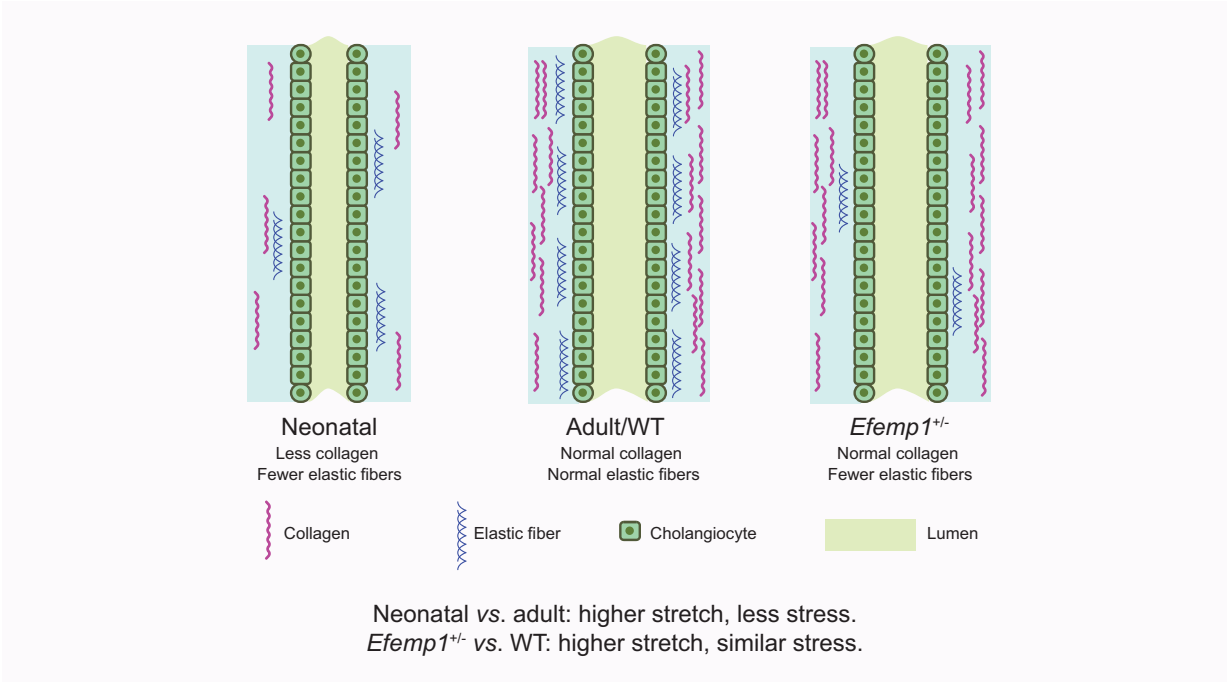

Neonatal *vs*. adult: higher stretch, less stress.
Efemp1$^{+/-}$ *vs*. WT: higher stretch, similar stress.

Highlights:

- Fibulin-3 regulates elastic fiber organization in extrahepatic bile ducts, impacting their mechanical properties.
- *Efemp1*$^{+/-}$ mice show disrupted elastic fiber alignment, highlighting the role of fibulin-3 in fiber organization.
- Pressure myography shows that neonatal EHBDs stretch more and are softer than adult EHBDs.
- This work links genetic predisposition to biliary atresia to mechanical dysfunction.

Impact and implications:

The gene EFEMP1 was found via a genome-wide association study to be a susceptibility gene for the neonatal disease biliary atresia. EFEMP1 encodes the protein fibulin-3, which regulates elastic fiber organization in the extrahepatic bile duct (EHBD), the major site of disease in biliary atresia. We showed that neonatal EHBDs as well as mice heterozygous for *Efemp1* have decreased numbers of elastic fibers, and that this alters EHBD mechanics. This work is important for understanding the mechanism of biliary atresia, in particular susceptibility to obstruction.

https://doi.org/10.1016/j.jhepr.2024.101215

Research article

JHEP|Reports

Biliary atresia susceptibility gene EFEMP1 regulates extrahepatic bile duct elastic fiber formation and mechanics

Kapish Gupta[1,2,†,#], **Jessica Llewellyn**[1,2,†], Emilia Roberts[3], Chengyang Liu[4], Ali Naji[4], Richard K. Assoian[2,3,5], Rebecca G. Wells[1,2,*]

JHEP Reports **2025**. vol. 7 | 1–10

Background & Aims: EGF-containing fibulin extracellular matrix protein 1 (EFEMP1, also called fibulin-3) is an extracellular matrix protein linked in a genome-wide association study to biliary atresia, a fibrotic disease of the neonatal extrahepatic bile duct. Fibulin-3 is deposited in most tissues and *Efemp1* null mice have decreased elastic fibers in visceral fascia; however, fibulin-3 does not have a role in the development of large elastic fibers and its overall function in the extrahepatic bile ducts remains unclear.

Methods: We used staining and histology to define the amount and organization of key extracellular matrix components in the extrahepatic bile ducts. We also repurposed pressure myography, a technique heretofore applied to the vasculature, to determine the contribution of elastin and fibulin-3 to extrahepatic bile duct mechanics. We examined extrahepatic bile duct structure and mechanics in three models: neonatal *vs.* adult rat ducts (n = 6 each), elastase-treated adult rat ducts (n = 6-7 each), and *Efemp1*$^{+/-}$ *vs.* wild-type mouse ducts (n = 6 each).

Results: We demonstrated that fibulin-3 is expressed in the submucosa of both neonatal and adult mouse, rat and human extrahepatic bile ducts and that, in adult *Efemp1*$^{+/-}$ mouse ducts, elastin organization into fibers is decreased by approximately half. Pressure myography showed that *Efemp1*$^{+/-}$ ducts have altered mechanics compared to control ducts, with *Efemp1*$^{+/-}$ ducts displaying significant stretch compared to controls (p = 0.0376); these changes in stretch are similar to those observed in elastase-treated *vs*. normal ducts (p <0.0001) and in neonatal ducts *vs.* adult ducts (p <0.0001).

Conclusion: Fibulin-3 has an important role in the formation of elastic fibers and the mechanical properties of the extrahepatic bile duct. This provides functional relevance for the biliary atresia susceptibility gene EFEMP1.

Introduction

Biliary atresia (BA) is a rare and severe pediatric disease that initially causes fibrosis, obstruction, and obliteration of the extrahepatic bile ducts (EHBDs) but then rapidly leads to liver fibrosis and end-stage liver disease. The pathogenesis of BA is poorly understood although the inciting event appears to be exposure to an environmental agent such as a toxin[1–5] or virus[6] during gestation of a fetus with developmental[7] and genetic susceptibility.[8,9]

We previously identified significant differences between the neonatal and adult mouse EHBD in cholangiocyte glycocalyx maturity and junctional permeability and in submucosal extracellular matrix (ECM) composition and fibroblast behavior.[10] Notably, neonatal EHBDs show decreased quantity and alignment of the key ECM fibrillar proteins elastin and collagen, indicating an underdeveloped structural framework compared to adults. However, the significance of these age-related differences in ductular mechanics or BA is unclear.

Genome-wide association studies (GWASs) have implicated matrix proteins including EGF-containing fibulin extracellular matrix protein 1 (EFEMP1) as susceptibility genes for BA.[8] EFEMP1, also known as fibulin-3, belongs to the fibulin family of proteins that contribute to ECM organization and stability. Fibulin-3 is part of the short fibulins subgroup. Its function is less well described than that of fibulins -4 and -5, which have critical roles in large vessel elastic fiber formation. Although fibulin-3 is expressed in tissues with large elastic fibers, such as the lung and aorta, these organs appear normal in *Efemp1*$^{-/-}$ mice.[11,12] Instead, *Efemp1*$^{-/-}$ mice display a loss of fine elastic fibers in the fascia with fascial herniation, early aging, and low reproductive capacity. This suggests that the function of fibulin-3 depends on the size of elastic fibers or on the tissue.[13] Fibulin-3 exhibits a weak binding affinity for tropoelastin but does not interact with fibrillin-1, the primary component of the microfibril that surrounds elastin.[11,14] Notably, electron microscopy analysis of *Efemp1*$^{-/-}$ mouse skin showed fragmented

* Corresponding author. Address: 421 Curie Boulevard, 905 BRB II/III, Philadelphia, PA 19104, United States; Tel.: 610 322-2627, fax: 215 573-2024.
E-mail address: rgwells@pennmedicine.upenn.edu (R.G. Wells).
† These authors contributed equally.
# Current address for Kapish Gupta: Department of Biosciences and Bioengineering Indian Institute of Technology Guwahati, Assam, India
https://doi.org/10.1016/j.jhepr.2024.101215

elastin cores within elastic fibers.[12] Given the changes in ECM composition during EHBD development and the association between EFEMP1 and BA, our goal was to define the role of EFEMP1 in the matrix and mechanics of the EHBD.

Materials and methods

Human tissue

Anonymized fresh human EHBD was obtained as part of the HPPAP (Human Pancreas Procurement and Analysis Program), which was granted IRB exemption (protocol 826489). Samples were taken after the unexpected deaths of otherwise healthy individuals, with consent obtained from next of kin. The samples were formalin-fixed and embedded after receipt.

Mouse tissue

All work with mice was in accordance with protocol 804862, approved by the University of Pennsylvania Institutional Animal Care and Use Committee, and followed the guidelines of the National Institutes of Health Guide for the Use and Care of Animals. For transparency, we have provided information following the ARRIVE guidelines 2.0. C57Bl/6j mice were obtained from the Jackson Laboratory (Bar Harbor, ME, USA). Three C57Bl/6j mice per age group (total of 18) were used to determine postnatal EFEMP1 expression. *Efemp1*$^{+/-}$ mice were a gift from Lihua Marmorstein (University of Arizona).[12] *Efemp1*$^{+/-}$ pairs were bred; however, although the nulls are reported to be viable, for unclear reasons only *Efemp1*$^{+/-}$ and *Efemp1*$^{+/+}$ offspring were born in our colony. In this study we compared *Efemp1*$^{+/-}$ mice to *Efemp1*$^{+/+}$ control littermates. Mice were kept on a 12 h light/12 h dark cycle with *ad libitum* access to standard chow and water. EHBDs were dissected from mice at different ages as noted in the figures and were formalin-fixed (10%), paraffin-embedded and sectioned at 5 μm thickness. For pressure myography (detailed below), EHBDs were isolated from adult (10–15-week-old) wild-type (WT; *Efemp1*$^{+/+}$) and *Efemp1*$^{+/-}$ mice.

Rat tissue

All rat experiments were conducted following National Institutes of Health policy, and the study was approved by the Institutional Animal Care and Use Committee at the University of Pennsylvania under protocol 804031. EHBDs were isolated from neonatal rats aged 7-10 days old and adult rats aged 3-6 months. We did not determine sex for individual animals given that anogenital distance measurements in pups lack accuracy, but our random selection typically yields a balanced male-female distribution. A subset of adult EHBDs were incubated with 1 U/ml elastase (Worthington Biochemical Corporation, Lakewood, NJ) or Hank's balanced salt solution (control) for 20 min at room temperature. Subsequently, the EHBDs were mounted onto the Pressure Myograph System and analyzed in accordance with the procedures detailed in under "Pressure Myography". Following pressure myography, EHBDs were formalin-fixed (10%), paraffin-embedded, sectioned at 5 μm thickness and stained.

Matrix imaging

For immunofluorescence of mouse and human EHBDs, samples were dewaxed with xylene and rehydrated through a graded series of alcohols and distilled water. Heat-mediated antigen retrieval with 10 mM citric acid pH 6.0 in a pressure cooker for 2 h was used for staining with antibodies against EFEMP1 (fibulin-3) (1:100, Thermo Fisher, Waltham, MA, #PA5-29347), fibulin-4 (1:100, Abcam, Waltham, MA, #Ab1250730), or fibulin-5 (1:200, Proteintech, Rosement, IL, #12188-1-AP). 0.5% hyaluronidase (Sigma, H3506 type I–S, St-Louis, MO) treatment for 60 min at 37 °C was used for staining with antibodies against elastin (1:100, Bioss, Woburn, MA, #bs-1756R). Sections were blocked with StartingBlock™ T20/phosphate buffered saline Blocking Buffer (Thermo Scientific, Waltham, MA) before being incubated with primary antibodies (in 0.2% Triton X-100, 3% serum, in phosphate buffered saline) at 4 °C overnight. Sections were then incubated with Cy3-conjugated anti-rabbit secondary antibody for 60 min (1:500, Vector Laboratories, Burlington, CA) and DAPI for 10 min (4', 6-Diamidino-2-Phenylindole, Dihydrochloride) and were mounted. Stained sections were imaged using a Zeiss Axio Observer 7 inverted microscope and ZEN blue software. For elastic fiber staining, paraffin sections were dewaxed and rehydrated and stained using an Elastic Stain Kit (Millipore, HT25A, Burlington, MA) and ELASTIN staining solution acc. to Weigert (Sigma) according to the manufacturer's protocol. Brightfield imaging was done on a Nikon E600 microscope with Nikon NIS-Elements software and a Leica Aperio Slide Scanner. For second harmonic generation (SHG) imaging, paraffin sections were imaged using a Leica SP8 confocal/multiphoton microscope and Coherent Chameleon Vision II Ti:Sapphire laser (Leica, Buffalo Grove, IL) tuned to a wavelength of 910 nm.

Image analysis

Raw image files from immunofluorescence and SHG imaging were processed using Fiji ImageJ software.[15] Quantification of the percent area stained was assessed using the threshold and percent area functions. The number of elastic fibers per 50 μm^2 was counted manually using the Count tool. The crimp wavelength and depth were measured manually using the Line tool as described in.[16] For all analyses, 3-5 images per sample were taken. The individual doing the crimp analysis was blinded to the identity of the sample.

Slides stained with ELASTIN staining solution acc. to Weigert were processed using QuPath v0.2.0 software. Elastin signal was segmented from brightfield images using the default color deconvolution method available in QuPath.[17] Segmented images were imported to Fiji ImageJ. Quantification of the percent area stained was assessed using the threshold and percent area functions.

Pressure myography

EHBDs were isolated and placed in Hank's balanced salt solution without calcium and magnesium at 37 °C. The cut ends of the EHBDs were then carefully threaded onto two 385 μm stainless steel cannulas on a DMT model 114P Pressure Myograph (DMT-USA, Ann Arbor, MI) and tied into place with 6-0 silk sutures (SUT-S 104, Braintree Scientific Inc., Braintree, MA), creating a closed system. The system was fitted with a Nikon Diaphot inverted microscope, enabling measurement of the vessel length, wall thickness and outer diameter using MYOVIEW software (DMT-USA, Ann Arbor, MI). The mounted ducts were stretched until straight, the force transducer was

brought to zero, and then the ducts were stretched axially to 1 mN of force to standardize baseline axial conditions. The system was pressurized using medical air (AI USP 300; Airgas USA, Cherry Hill, NJ) and the EHBDs were preconditioned for 15 min at 40 mmHg before being pressurized in a stepwise manner from 0-20 mmHg in 2 mmHg increments. This was done 3 times on each EHBD and values were averaged for data analysis. The pressure myography testing and data collection were carried out blinded (the individual carrying out the measurements was blinded to the genotype, and for the analysis was blinded to the genotype and age of the sample) and the sequence of testing for control *vs.* test ducts was done randomly to avoid any confounding effects. Axial stretch measurements were not performed as these are unlikely to be forces experienced by the EHBD due to the low pressure of the system. Real-time imaging and MYOVIEW software were used for direct measurement of the loaded outer diameters ($2a_o$). From this, the unloaded inner radius (A_i) was calculated as A_i=A_0-H, where A_0 is the unloaded outer radius and H is the unloaded wall thickness. The duct volume (V) determined based on unloaded diameter and wall thickness was used to determine the loaded inner radius using $a_i = \sqrt{a_0^2 - (V/\pi l)}$ where l is the length between the inner sutures, measured using calipers. The loaded wall thickness (h) was calculated using h=a_0-a_i. The circumferential stretch (λ_θ) was calculated using λ_θ= (a_i + h/2)/(A_I+H/2) and circumferential stress using σ_θ= (Pa_i)/h where P is pressure. Because the EHBD shows a nonlinear stress-stretch relationship, the tangent modulus (slope) was calculated as a measure of EHBD stiffness. An exponential curve was fitted to the stress-stretch curve using MATLAB (R2021a, curve fitting tool) and the tangent modulus was obtained by taking the derivative of the stress-stretch curves.

Statistical analysis

Statistical significance was calculated with Prism 10 (GraphPad software, LaJolla, CA). The image analysis data were assessed by unpaired t-test for data that were normally distributed. When the data were not normally distributed, the Mann-Whitney test was used. Statistical significance of the pressure myography individual parameters (outer diameter, stretch and stress) was assessed using a mixed-effects model with repeated measures to assess the effect of age, elastase treatment or genotype. All data are shown as mean ± SEM.

Results

Fibulin-3 regulates elastic fiber formation

To understand the contribution of fibulin-3 to the ECM of the EHBD, we characterized key components of ECM found in the submucosa of adult *Efemp1*$^{+/-}$ mice. We first found that *Efemp1*$^{+/-}$ mice have a significant (>50%) reduction in submucosal fibulin-3 expression, with levels of fibulin -4 and -5 unchanged from controls (Fig. S1). The fibulin-3 that was present was disproportionately found in the cholangiocyte (biliary epithelial cell) cytoplasm rather than the submucosa (Fig. S1). Previous studies have documented the presence of fibulins in both cytoplasmic and extracellular compartments.[18] It has been reported using cultured cells that intracellular fibulin was detected early after plating, but extracellular fibulin secretion did not occur until after 4 h.[19]

To assess the impact of fibulin-3 on ECM organization, we compared the presence and organization of collagen, elastin, and elastic fibers in EHBDs from *Efemp1*$^{+/-}$ and WT littermate mice. The amount of elastin in the submucosa of the EHBD was comparable between WT and *Efemp1*$^{+/-}$ mice (Fig. 1A,B). In WT mice, elastin was localized beneath the cholangiocyte monolayer. However, in *Efemp1*$^{+/-}$ mice, the deposition of elastin was more diffuse and its concentration under the cholangiocyte layer less pronounced, suggesting that fibulin-3 has no effect on the deposition of elastin but plays an important role in its organization. In line with this, the number of elastic fibers in the EHBD submucosa was significantly reduced in *Efemp1*$^{+/-}$ mice compared to WT, suggesting that fibulin-3 plays a role in elastic fiber formation without impacting elastin expression (Fig. 1C,D and Fig. S2). To determine whether this disruption was unique to elastin, the amount and hallmark crimp of collagen were also assessed. Collagen was visualized using SHG imaging, which showed that both the amount of collagen present (Fig. 1E,F) and the crimp pattern (Fig. S3) were unaltered in *Efemp1*$^{+/-}$ mice compared to WT mice. These data suggest a specific role for fibulin-3 in the organization of ECM in the EHBD and in the formation of elastic fibers.

The structure of the EHBD differs between neonates and adults

We then assessed the expression patterns of fibulin-3 during postnatal development in both mouse and human EHBDs (Fig. 2 and Figs S4,S5). In the neonatal (P2) mouse EHBD, fibulin-3 was expressed in both cholangiocytes and fibroblasts. However, in adult EHBDs, fibulin-3 primarily accumulated in the EHBD submucosa, with limited intracellular expression (Fig. 2A and Fig. S4). In human EHBDs, fibulin-3 also showed increased expression in the submucosa with increasing age (Fig. S5). To further investigate the potential role of fibulin-3 in elastic fiber formation during postnatal development, we stained for both elastin and elastic fibers in mice (Fig. 2B,C and Fig. S6). Elastin deposition was first detectable at P5, while elastic fibers became visible between P10 and P14 (Fig. 2B,C). In adult EHBDs, fibulin-3, elastin, and elastic fibers were deposited robustly under the cholangiocyte layer, although they were also present throughout the EHBD submucosa (Fig. 2 and Figs. S4–6); fibulin-3 was not visible in cholangiocytes at any time point in humans, although we did not evaluate fetal human EHBDs. The sequential presence and similar distribution are consistent with a role for fibulin-3 in elastic fiber formation, as shown in *Efemp1*$^{+/-}$ mice (Fig. 1).

The mechanics of the EHBD differ between neonates and adults

We determined the functional relevance of fibulin-3 with pressure myography. This method is often used to measure blood vessel mechanical responses to pressure, specifically changes in vessel dimensions and cross-sectional area,[20–23] which enable the calculation of circumferential wall stress and strain under increasing pressure, where stress reflects the force experienced by the vessel and strain represents relative changes in vessel dimension. While stress and strain can be used to quantify vessel stiffness, the stress-strain relationship in tissue is typically nonlinear and an incremental (tangent) elastic modulus is therefore obtained by fitting the stress-strain curve to an exponential curve and determining the derivative.

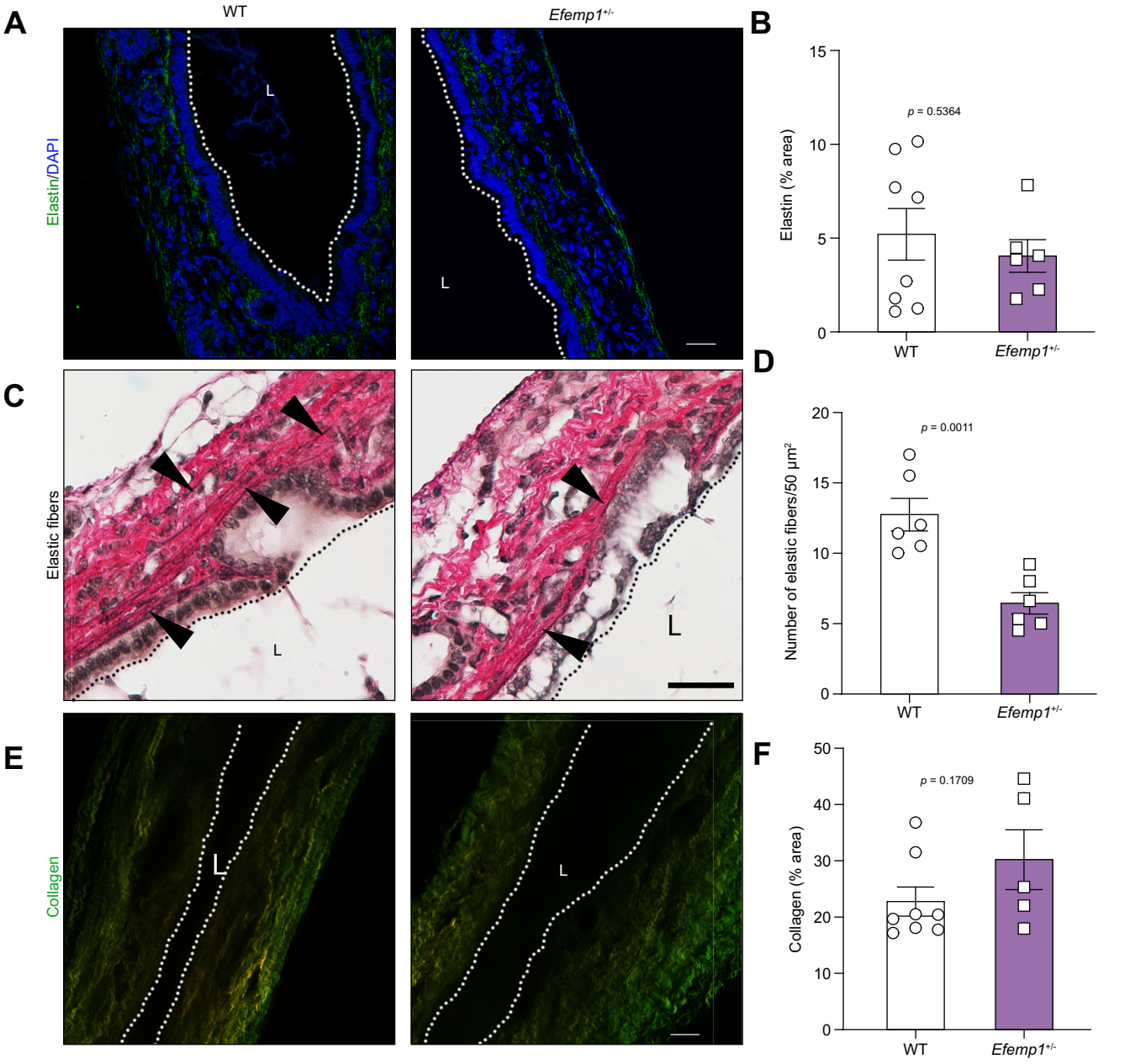

Fig. 1. Elastic fibers are reduced in adult *Efemp1*$^{+/-}$ EHBDs but elastin expression is unchanged. (A) Representative staining of elastin in WT and *Efemp1*$^{+/-}$ EHBDs. (B) Quantification of percent area of staining. (C) Representative elastic fiber staining of WT and *Efemp1*$^{+/-}$ EHBDs. Arrowheads show examples of elastic fibers. Note organized fibers under the basement membrane in WT. Additional examples shown in Fig. S2. (D) Quantification of the number of elastic fibers per 50 µm^2. (E) Representative images of collagen by SHG imaging in WT and *Efemp1*$^{+/-}$ EHBDs. (F) Quantification of percent collagen area of SHG signal. Forward signal in red and backward signal in green. Dotted lines and L denote lumens. 6-8 ducts were analyzed per genotype for all stains, with 3-5 images taken per duct. All scale bars 50 µm. Data shown are mean ± SEM. Significance in B and D determined by unpaired t-test. Significance in F determined using the Mann-Whitney test since the data were not normally distributed. EHBD, extrahepatic bile duct; SHG, second harmonic generation; WT, wild-type.

These measurements in blood vessels serve as a predictors for cardiovascular events, offering insights into overall cardiovascular health. We reasoned that the ductular structure of the EHBD would be amenable to this technique as well and would provide insight into the functional mechanics of the duct.

We first compared neonatal and adult EHBDs. Neonatal mouse EHBDs are too small for pressure myography, so we used rat EHBDs, first confirming that rat and mouse EHBDs have similar developmental patterns of collagen and elastin deposition (Fig. S7). We found that with the application of increasing luminal pressure to ducts, there was rapid elastic expansion of the lumen up to 8 mmHg, after which expansion slowed (Fig. 3B). Circumferential stretch and circumferential stress were calculated using the changes in lumen diameter and wall thickness with pressure (Fig. 3C,D), as described in the Methods. Neonatal ducts experienced less stress (Fig. 3C) but displayed more stretch (Fig. 3D). This increased stretch is most evident in the initial pressurization of the lumen from an

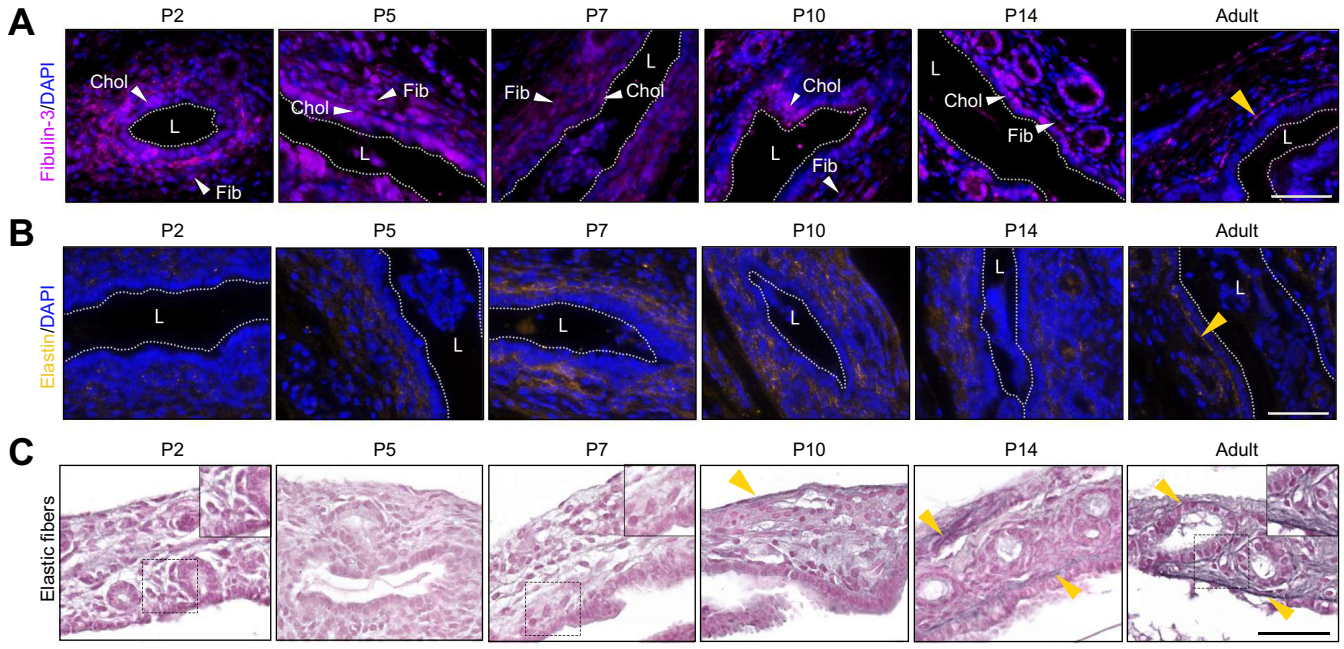

Fig. 2. Fibulin-3 expression and elastin organization during postnatal development of the mouse EHBD. (A) Representative images of fibulin-3 staining in neonatal (P2, 5, 7, 10, 14) and adult mouse EHBD. White arrows show cholangiocytes (Chol) and likely fibroblasts (Fib) expressing fibulin-3. Yellow arrow shows fibulin-3 localization under the cholangiocyte monolayer in adult. (B) Representative images of elastin staining in mouse samples. Yellow arrow shows elastin localization under the cholangiocyte monolayer in the adult EHBD. In all immunohistochemistry stains, nuclei are stained with DAPI (blue). For A and B, in all images, dotted lines and L denote lumens. (C) Representative images of elastic fiber staining. Yellow arrows show elastic fiber localization under the cholangiocyte monolayer. Images in insets show regions highlighted in boxes outlined with dotted lines. 3-4 samples were stained for each age, with 3-5 images taken per duct. EHBD, extrahepatic bile duct.

unloaded state (0 mmHg) to a physiologically relevant pressure (2 mmHg) (Fig. 3E). The stress and stretch curves show that neonatal ducts have a different profile than adult ducts, with the neonatal ducts experiencing more stretch at lower stress compared to adults. The stress-stretch curve (Fig. 3F) was used to determine the incremental tangent modulus, a metric used to describe the "stiffness" of a tissue; this was lower in neonates than adults (Fig. 3G).

Disruption of elastic fibers by elastase treatment leads to altered mechanics

The differences in mechanical properties between neonatal and adult EHBDs are likely due to differences in collagen and elastin (Figs 2, 3B and Fig. S7). The literature suggests that, at least in the vasculature, mechanics measured by pressure myography are determined by these two structural proteins and the response to filling occurs in two phases, the initial phase determined by elastin and the second phase by collagen, as illustrated in Fig. 3B.[23] To determine whether elastic fibers play a similar role in EHBD mechanics as in vascular mechanics, rat EHBDs were treated with elastase to break down elastic fibers before pressure myography. Concentration and length of treatment were optimized to ensure that elastic fibers were disrupted (Fig. 4A,B), but ducts remained structurally able to withstand pressure myography testing. We observed that elastase-treated EHBDs had a very different outer diameter response profile than control ducts (Fig. 4C) and that elastase-treated ducts experienced significantly higher stress and stretch. Stretch plateaued at 2 mmHg (Fig. 4D-F), at which point the inner radius of elastase-treated EHBDs showed a significant increase (180%) compared to a non-significant increase in control EHBDs (Fig. 4F). This resulted in a marked shift of the stress-stretch curve to the right and upwards, with a significantly higher incremental tangent modulus (Fig. S8). Given that the changes in the mechanics occurred due to significant lumen expansion at low pressure, these results suggest that the initial phase of lumen expansion in the EHBD is regulated by elastin in a manner similar to blood vessels.

Efemp1$^{+/-}$ EHBDs show disrupted mechanics suggestive of decreased elastic fibers

Having observed that EHBDs from *Efemp1*$^{+/-}$ mice have fewer elastic fibers than their WT littermates, we compared the response of adult *Efemp1*$^{+/-}$ and WT littermate EHBDs. The outer diameter of *Efemp1*$^{+/-}$ ducts increased more than the outer diameter of WT ducts at low pressure; however, the overall outer diameter curves were not significantly different (Fig. 5A). The stress experienced by WT and *Efemp1*$^{+/-}$ EHBDs was also comparable (Fig. 5B). However, *Efemp1*$^{+/-}$ EHBDs showed significantly higher stretch than WT EHBDs (Fig. 5C). This is likely because the stretch is calculated using the inner diameter. As the pressure increased, the outer diameter increased and the wall thickness of the duct decreased, but this occurred at different rates in the *Efemp1*$^{+/-}$ and WT ducts; the change in inner diameter between 0 mmHg and 2 mmHg was significantly higher in *Efemp1*$^{+/-}$ ducts (45% increase, p = 0.0106) than in WT (10% increase, not statistically significant) (Fig. 5D). Given that the stretch profile was significantly altered without a significant change in stress, the incremental tangent modulus (stiffness) profile was higher in *Efemp1*$^{+/-}$ mice

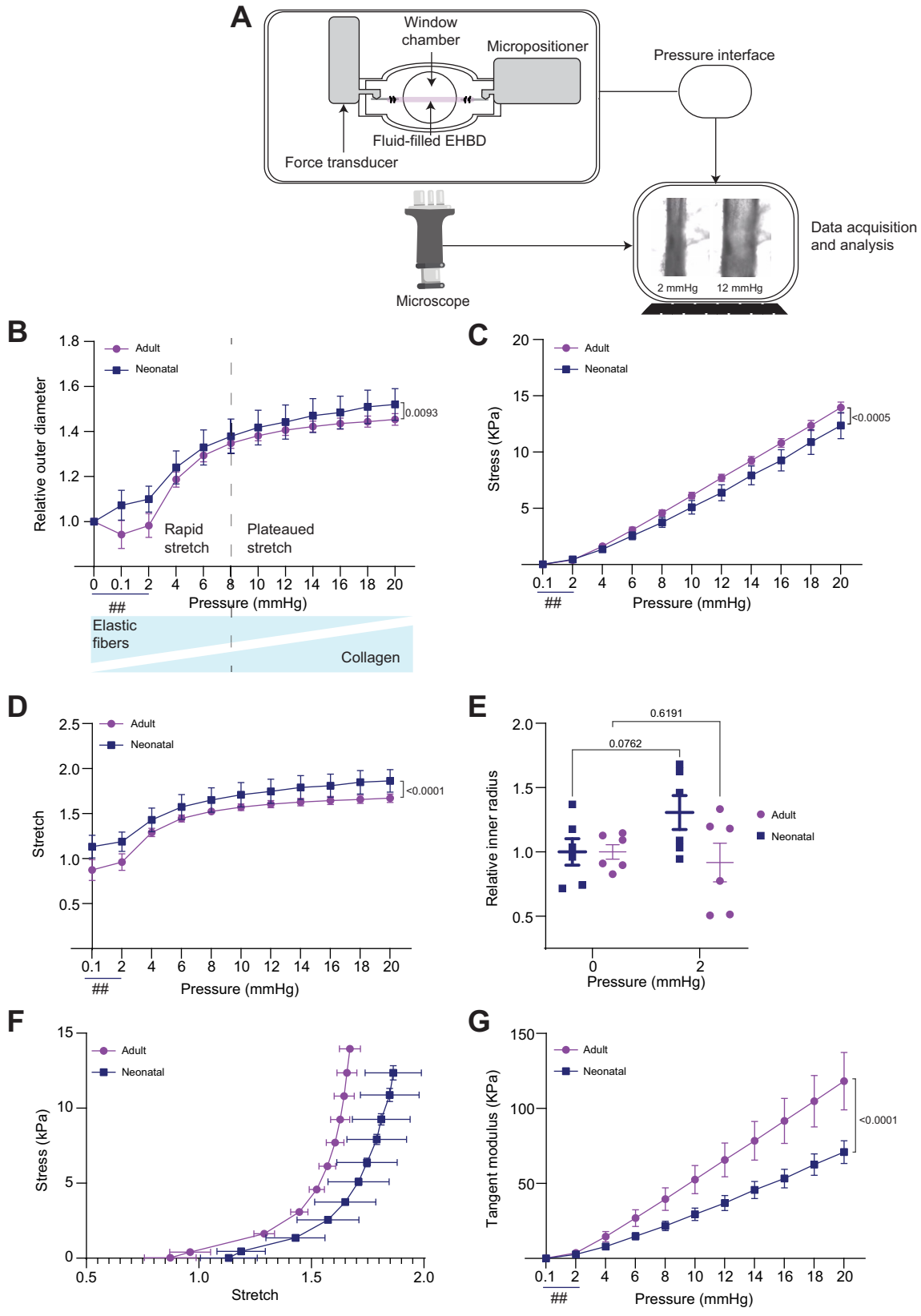

Fig. 3. Neonatal and adult rat EHBDs have different mechanics. (A) Schematic of the pressure myography setup. The EHBD is mounted onto a pressure myography apparatus and progressively pressurized. A force transducer and micro-positioner control the pressure and position. The EHBD is imaged through a window chamber, and the data, including pressure values and microscopic images, is recorded and analyzed on a computer. (B) Relative outer diameter of neonatal (P7-10) and adult rat EHBDs at increasing pressures. Rapid stretch was observed up to 8 mmHg pressure followed by a plateau phase. Blue triangles under graph represent estimate of the

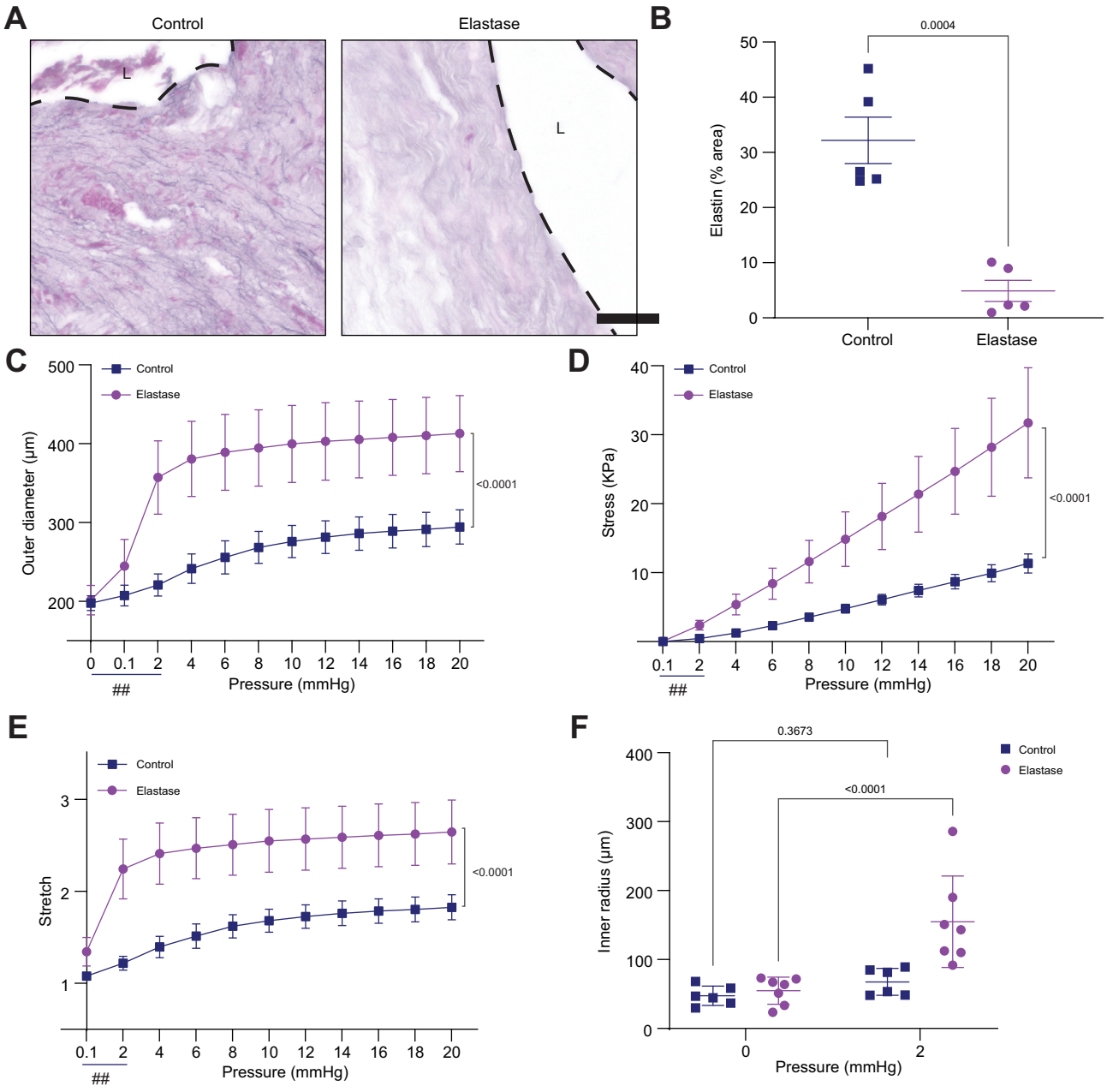

Fig. 4. Elastase treatment leads to altered EHBD mechanics. (A) Representative images of elastic fiber staining in control- and elastase-treated rat adult EHBDs stained using elastin staining solution according to Weigert. Dotted lines and L denote lumens. Scale bar, 50 µm. (B) Quantification showing significant removal of elastin after elastase treatment. (C) Measured outer diameter of control and elastase-treated rat EHBDs at increasing pressures. (D) Circumferential stress profile of control *vs.* elastase-treated EHBD. (E) Circumferential stretch profile of control *vs.* elastase-treated EHBD. (F) Relative change in inner radius of control *vs.* elastase-treated EHBD as pressure is increased from unloaded (0 mmHg) condition to physiological pressure (2 mmHg). Data shown are mean ± SEM. Six to seven rats used per condition. ## indicate uneven x axes. *p* value in graph B represents *p* value for t-test, in graph C-E represents two-way ANOVA between profile of elastase-*vs.* control-treated EHBD and in F represents Fisher's least significant difference after two-way ANOVA. EHBD, extrahepatic bile duct.

relative contribution of elastin and collagen to the curves, consistent with data from the vascular literature. (C) Circumferential stress profile of neonatal *vs.* adult EHBD. (D) Circumferential stretch profile of neonatal *vs.* adult EHBD as pressure is increased. (E) Relative change in inner radius of neonatal and adult EHBD as pressure is increased from unloaded (0 mmHg) to physiological pressure (2 mmHg). (F) Calculated circumferential stress and circumferential stretch of neonatal and adult EHBD under increasing pressure from unloaded (0 mmHg) to physiological pressure (2 mmHg). Statistical analyses for circumferential stress and circumferential stretch individually are shown in panels B and C. (G) Calculated tangent modulus (stiffness) of neonatal and adult rat EHBDs. Six individual ducts were examined per group. Note uneven x axes represented by ##. Data shown are mean ± SEM. *p* values in graphs B-D and G represent two-way ANOVA between neonatal and adult EHBD. *p* values in E represent Fisher's least significant difference after two-way ANOVA. EHBD, extrahepatic bile duct.

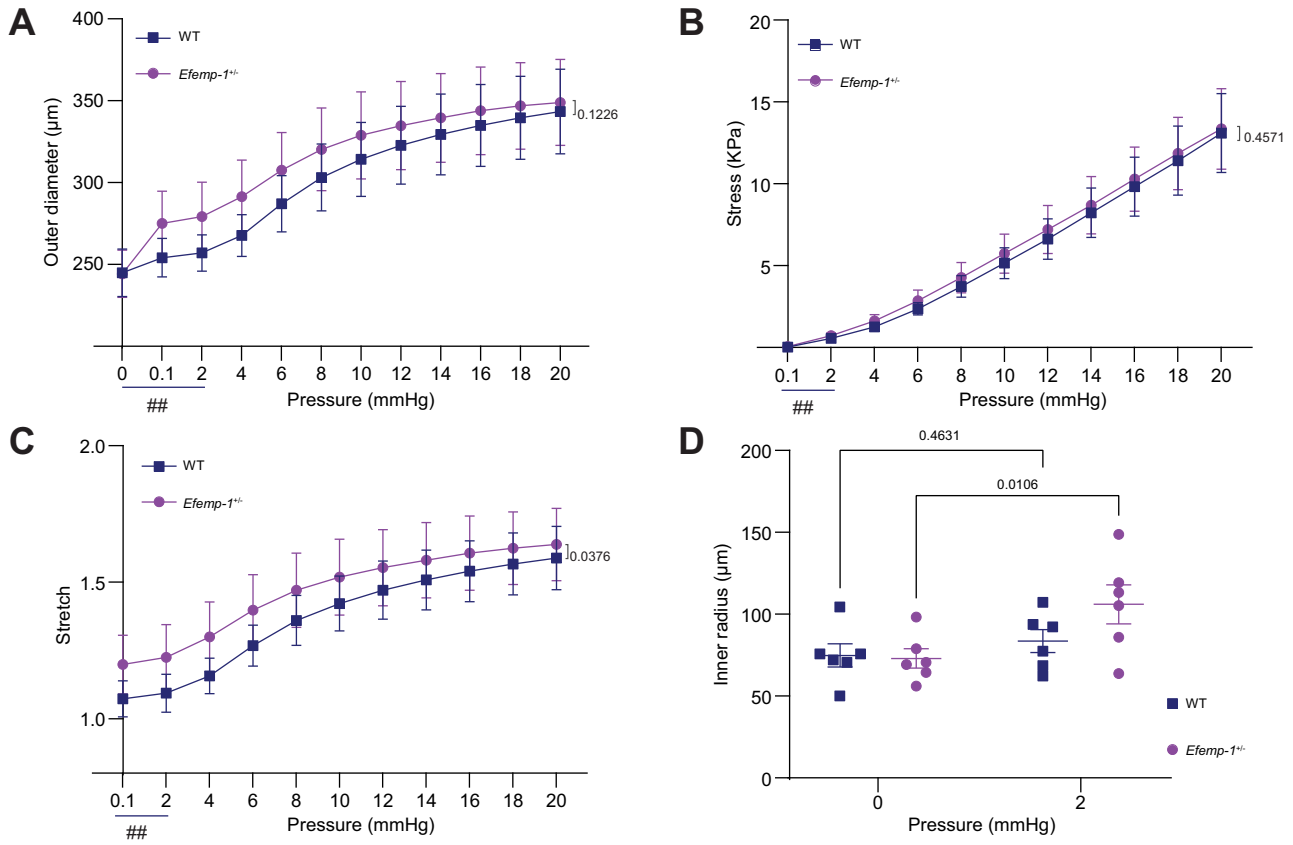

Fig. 5. Mechanical properties measured by pressure myography are altered in *Efemp1*$^{+/-}$ EHBDs. (A) Measured outer diameter of WT and *Efemp1*$^{+/-}$ adult mice EHBDs at increasing pressures. (B) Calculated circumferential stress of WT and *Efemp1*$^{+/-}$ adult mice EHBDs at increasing pressures. (C) Calculated circumferential stretch of WT and *Efemp1*$^{+/-}$ adult mice EHBDs at increasing pressures. (D) Relative change in inner diameter of WT *vs.* *Efemp1*$^{+/-}$ treated EHBD as pressure is increased from unloaded (0 mm Hg) condition to physiological pressure (2 mmHg). Data shown are mean ± SEM. Six mice used per condition. ## represent uneven x axes. *p* values in graphs A-C represent two-way ANOVA between profile of WT *vs.* *Efemp1*$^{+/-}$. *p* value in D represents Fisher's least significant difference after two-way ANOVA. EHBD, extrahepatic bile duct; WT, wild-type.

(Fig. S9). These experiments demonstrate that fibulin-3, acting via its effects on elastic fibers, has a functional role in EHBD mechanics, in particular the circumferential stretch response to physiological (1-2 mm Hg) filling pressures.

Discussion

We show here that fibulin-3, a protein implicated in ECM organization and encoded by the GWAS-identified BA susceptibility gene EFEMP1,[8] plays a significant role in elastic fiber organization in the EHBD and thereby in the EHBD response to filling pressure. Our work provides a plausible role for EFEMP1 in susceptibility to BA, making it one of the few BA susceptibility genes to have undergone some level of functional characterization.

Our study is notable in that we used pressure myography, a technique previously applied exclusively to blood vessels, to investigate the mechanical response of the EHBD to pressure and to document changes with age, elastase treatment, and heterozygous deletion of *Efemp-1*. The EHBD operates under low pressure *in vivo* (3-5 mmHg in humans[24,25]) when compared with arterial systems, as suggested by the absence of a thick elastic lamella or a smooth muscle layer. We therefore used significantly lower pressures for the EHBD than are typically used for arteries, designating 0.1 and 2 mmHg as representative of normal/physiological pressure and greater than 10 mmHg as indicative of obstructive pressure, consistent with physiological pressures of 0.8 and obstructive pressures of 10 mmHg reported for mice and rats[26,27] and 15-30 mmHg for humans.[24,25] Although changes in duct pressure with age have not been fully defined, it is likely that pressures are lower in neonates given the progressive increase in bile secretion after birth.

Because neonatal mice, like *Efemp1*$^{+/-}$ mice, have fewer elastic fibers than WT adults, we first used pressure myography to determine the differences in mechanical responses between neonates and adults. It was not possible to use *Efemp1*$^{-/-}$ mice given that they were not viable in our colony; however, a decrease as opposed to complete elimination of the protein may better replicate the impact of the human polymorphism. We observed that neonatal EHBDs experience higher stretch even though they experience less stress, which results in overall lower stiffness, with the most pronounced differences at a physiological pressure (2 mmHg). Additionally, there was a greater relative change in inner diameter of neonatal compared with adult ducts. This is probably because neonates exhibit an underdeveloped ECM characterized by sparse elastin and collagen fibers, as evident from our staining data.

It is noteworthy that, despite the relatively low-pressure nature of the EHBD, the degree of stretch experienced by EHBDs falls within the same range as arteries (stretch less than 2-fold). Furthermore, both EHBDs and arteries exhibit similar biphasic

stress-strain curves. In arterial systems, this initial phase is attributed to elastin contribution, while the subsequent phase is influenced by collagen.[23,28] We showed that pre-treatment of adult rat ducts with elastase led to stretch greater than 2 even at a pressure as low as 2 mmHg, demonstrating that the initial phase of the EHBD response, like that of arteries, is governed by elastin. The stretch response for elastase-treated ducts plateaued after reaching 2 mmHg, which resulted in the EHBDs exhibiting a significantly higher incremental tangential stretch. A similar increase in incremental tangential stiffness after elastase treatment has also been observed in arteries.[29]

We modified the measurement approach reported for arteries to be more suitable for EHBD, which is a low-rather than high-pressure system. In pressure myography studies of arteries, a pressure of ~3-10 mmHg is used as the starting pressure, which leads to significant differences in starting diameter between elastase-treated and control vessels and results in an overall leftward shift of the stress-stretch curve.[29,30] For ducts, we used the unloaded state as a starting point for measurement so that the starting diameters were similar in elastase-treated and control groups; this led to a rightward shift in the stress-stretch curve (Fig. S8A). The tangent modulus is calculated for the points across the entire curve.

We showed that, compared to WT mice, *Efemp1*$^{+/-}$ mice have a defect in the organization of elastin into elastic fibers. As we found for adult rat ducts treated with elastase, the difference in stretch between ducts from *Efemp1*$^{+/-}$ *vs.* WT animals occurred in the low-pressure phase, with a 45% increase in the luminal inner radius found for *Efemp1*$^{+/-}$ in the loaded (2 mmHg) state compared to the unloaded state. Comparative analysis of the stress-stretch curves for WT and *Efemp1*$^{+/-}$ ducts showed a clear difference in stretch (Fig. S9A), which we attribute to changes in elastin fibers. The similar shifts in elastase-treated and *Efemp1*$^{+/-}$ mice compared to untreated/WT controls highlights the role of fibulin-3 in elastin organization. We also observed an increase in stiffness, a hallmark of many diseases, in the *Efemp1*$^{+/-}$ ducts (Fig. S9B). Although the role of stiffness in duct diseases is not known, it is likely that increased stiffness could hinder bile flow at higher pressures, particularly if there is partial obstruction.[31] Overall, our findings suggest that fibulin-3 modulates EHBD responses to physiological levels of mechanical stress.

The data suggest that the EHBD experiences significant stretch even under physiological pressures, potentially impacting both cholangiocytes and interstitial fibroblasts. Neonatal EHBD cholangiocytes, in particular, have immature tight junctions[10] such that heightened stretch, as observed in the context of fibulin-3 abnormalities, could predispose them to the leakage of toxic bile into the submucosa, thereby inducing injury.[32] Increased stretch could also affect submucosal fibroblasts, known for their high mechanosensitivity.[33,34] Additionally, elevated stretch could influence the ability of cholangiocytes to counteract oxidative stress. Emerging evidence suggests that an immature antioxidant system in neonates, coupled with possible oxidative stress, plays a crucial role in BA pathogenesis.[1,3,31,35,36] Stretch-induced production of reactive oxygen species at physiological pressures might render cholangiocytes more susceptible to BA.

Multiple genes have been identified by GWAS as being BA susceptibility genes, including several linked to "biliary development and structure", but the functional ramifications for EHBD function are generally only vaguely understood.[37] The specific effects of EFEMP1 polymorphisms on fibulin-3 expression were not identified in the GWAS study that originally linked EFEMP1 to BA, and levels of fibulin-3 were not measured in the EHBDs from controls or patients with BA. Our work here (see especially Fig. 2) suggests that a detailed study of fibulin-3 and elastic fiber organization in the EHBD submucosa in early BA will be necessary to fully understand the relationship between fibulin-3 and BA. We recently suggested that EHBD obstruction, potentially related to a program of fetal wound healing, is a critical step in the pathophysiology of BA.[7,31] In this context, the demonstration in this work that fibulin-3 alters the EHBD response to pressures typical of obstruction provides a reasonable explanation for EFEMP-1 as a BA susceptibility gene.

In conclusion, we use a novel application of pressure myography to provide a compelling mechanism explaining the role of EFEMP1 as a BA susceptibility gene. Our data suggest that decreased levels of fibulin-3 impair the ability of the EHBD to respond to potential luminal narrowing, as can occur in response to an injury. Future work will need to focus on the role of obstruction in BA, particularly early, and on the potential modifying effects of fibulin-3 in humans.

Affiliations

[1]*Division of Gastroenterology and Hepatology, Department of Medicine, University of Pennsylvania, Philadelphia, PA, USA;* [2]*Center for Engineering MechanoBiology, University of Pennsylvania, Philadelphia, PA, USA;* [3]*Program in Translational Biomechanics, Institute for Translational Medicine and Therapeutics, University of Pennsylvania, PA, USA;* [4]*Department of Surgery, University of Pennsylvania, PA, USA;* [5]*Department of Systems Pharmacology and Translational Therapeutics, University of Pennsylvania, PA, USA*

Abbreviations

BA, biliary atresia; ECM, extracellular matrix; EFEMP1, EGF-containing fibulin extracellular matrix protein 1; EHBD, extrahepatic bile duct; GWAS, genome-wide association study; SHG, second harmonic generation; WT, wild-type.

Financial support

E.R. was supported by the Program in Translational Biomechanics of the Institute for Translational Medicine and Therapeutics at the University of Pennsylvania. Funding was provided by NIH R01 DK119290 (to R.G.W.); NIH grant UC4 DK112217 (to A.N.) and the NIDDK/City of Hope Integrated Islet Distribution Program (IIDP) Inst. #10039645; the Center for Engineering MechanoBiology (CEMB), an NSF Science and Technology Center, under grant agreement CMMI: 15-48571 (to R.G.W. and R.K.A.); and the Fred and Suzanne Biesecker Pediatric Liver Center (to R.G.W.). The study was also supported by NIH grant AG062140 to R.K.A.

Conflict of interest

The authors declare no conflict of interest.

Please refer to the accompanying ICMJE disclosure forms for further details.

Authors' contributions

Kapish Gupta: Conceptualization, Formal analysis, Methodology, Investigation, Writing - original draft. Jessica Llewellyn: Conceptualization, Formal analysis, Methodology, Investigation, Writing - original draft. Emilia Roberts: Formal analysis, Methodology. Chengyang Liu: Methodology.

Ali Naji: Methodology. Richard K. Assoian: Conceptualization, Resources, Funding acquisition, Supervision, Writing - review & editing. Rebecca G. Wells: Conceptualization, Resources, Funding acquisition, Supervision, Writing - review & editing.

Data availability statement

The data that support the findings of this study are available from the corresponding author upon reasonable request.

Acknowledgements

We thank Lihua Y. Marmostein (University of Arizona) for the gift of Efemp1+/- mice. We gratefully acknowledge the assistance of the following core facilities and individuals at the University of Pennsylvania: the Penn Vet Imaging Core (NIH S10 OD021633) and Gordon Ruthel, the Perelman School of Medicine Cell and Developmental Biology Microscopy Core, and the NIDDK Center for Molecular Studies in Digestive and Liver Diseases Molecular Pathology and Imaging Core (NIH P30 DK050306).

Supplementary data

Supplementary data to this article can be found online at https://doi.org/10.1016/j.jhepr.2024.101215.

References

Author names in bold designate shared co-first authorship

[1] Gupta K, Chen D, Wells RG. Microcystin-RR is a biliary toxin selective for neonatal cholangiocytes. JHEP Reports 2024:101218. https://doi.org/10.1016/j.jhepr.2024.101218.
[2] **Lorent K**, **Gong W**, **Koo KA**, et al. Identification of a plant isoflavonoid that causes biliary atresia. Sci Transl Med 2015;7:286ra67. https://doi.org/10.1126/scitranslmed.aaa1652.
[3] Zhao X, Lorent K, Wilkins BJ, et al. Glutathione antioxidant pathway activity and reserve determine toxicity and specificity of the biliary toxin biliatresone in zebrafish. Hepatology 2016;64:894–907. https://doi.org/10.1002/hep.28603.
[4] Koo KA, Lorent K, Gong W, et al. Biliatresone, a reactive natural toxin from dysphania glomulifera and D. littoralis: discovery of the toxic moiety 1,2-Diaryl-2-propenone. Chem Res Toxicol 2015;28:1519–1521. https://doi.org/10.1021/acs.chemrestox.5b00227.
[5] Gupta K, Xu JP, Diamond T, et al. Low-dose biliatresone treatment of pregnant mice causes subclinical biliary disease in their offspring: evidence for a spectrum of neonatal injury. PLoS One 2024;19:e0301824. https://doi.org/10.1371/journal.pone.0301824.
[6] Averbukh LD, Wu GY. Evidence for viral induction of biliary atresia: a review. J Clin Transl Hepatol 2018;6:410–419. https://doi.org/10.14218/JCTH.2018.00046.
[7] de Jong IEM, Hunt ML, Chen D, et al. A fetal wound healing program after intrauterine bile duct injury may contribute to biliary atresia. J Hepatol 2023;79:1396–1407. https://doi.org/10.1016/j.jhep.2023.08.010.
[8] **Chen Y**, **Gilbert MA**, Grochowski CM, et al. A genome-wide association study identifies a susceptibility locus for biliary atresia on 2p16.1 within the gene EFEMP1. PLoS Genet 2018;14:e1007532. https://doi.org/10.1371/journal.pgen.1007532.
[9] Ningappa M, Min J, Higgs BW, et al. Genome-wide association studies in biliary atresia. Wiley Interdiscip Rev Syst Biol Med 2015;7:267–273. https://doi.org/10.1002/wsbm.1303.
[10] **Khandekar G**, **Llewellyn J**, Kriegermeier A, et al. Coordinated development of the mouse extrahepatic bile duct: implications for neonatal susceptibility to biliary injury. J Hepatol 2020;72:135–145. https://doi.org/10.1016/j.jhep.2019.08.036.
[11] Kobayashi N, Kostka G, Garbe JHO, et al. A comparative analysis of the fibulin protein family: Biochemical characterization, binding interactions, and tissue localization. J Biol Chem 2007;282:11805–11816. https://doi.org/10.1074/jbc.M611029200.
[12] McLaughlin PJ, Bakall B, Choi J, et al. Lack of fibulin-3 causes early aging and herniation, but not macular degeneration in mice. Hum Mol Genet 2007;16:3059–3070. https://doi.org/10.1093/hmg/ddm264.
[13] Livingstone I, Uversky VN, Furniss D, et al. The pathophysiological significance of fibulin-3. Biomolecules 2020;10:1–24. https://doi.org/10.3390/biom10091294.
[14] El-Hallous E, Sasaki T, Hubmacher D, et al. Fibrillin-1 interactions with fibulins depend on the first hybrid domain and provide an adaptor function to tropoelastin. J Biol Chem 2007;282:8935–8946. https://doi.org/10.1074/jbc.M608204200.
[15] Schindelin J, Arganda-Carreras I, Frise E, et al. Fiji: an open-source platform for biological-image analysis. Nat Methods 2012;9:676–682. https://doi.org/10.1038/nmeth.2019.
[16] **Llewellyn J**, **Fede C**, Loneker AE, et al. Glisson's capsule matrix structure and function is altered in patients with cirrhosis irrespective of aetiology. JHEP Rep 2023;5:100760. https://doi.org/10.1016/j.jhepr.2023.100760.
[17] Ruifrok AC, Johnston DA. Quantification of histochemical staining by color deconvolution. Anal Quant Cytol Histol 2001;23:291–299.
[18] **Shi W-Q**, **Wan T**, Li B, et al. EFEMP1 is a potential biomarker of choroid thickness change in myopia. Front Neurosci 2023;17:1144421. https://doi.org/10.3389/fnins.2023.1144421.
[19] Argraves WS, Tran H, Burgess WH, et al. Fibulin is an extracellular matrix and plasma glycoprotein with repeated domain structure. J Cell Biol 1990;111:3155–3164. https://doi.org/10.1083/jcb.111.6.3155.
[20] Brankovic SA, Hawthorne EA, Yu X, et al. MMP12 deletion preferentially attenuates axial stiffening of aging arteries. J Biomech Eng 2019;141. https://doi.org/10.1115/1.4043322.
[21] Wenceslau CF, McCarthy CG, Earley S, et al. Guidelines for the measurement of vascular function and structure in isolated arteries and veins. Am J Physiol - Hear Circ Physiol 2021;321:H77–H111. https://doi.org/10.1152/ajpheart.01021.2020.
[22] Mulvany MJ, Halpern W. Contractile properties of small arterial resistance vessels in spontaneously hypertensive and normotensive rats. Circ Res 1977;41:19–26. https://doi.org/10.1161/01.RES.41.1.19.
[23] Wagenseil JE, Mecham RP. Elastin in large artery stiffness and hypertension. J Cardiovasc Transl Res 2012;5:264–273. https://doi.org/10.1007/s12265-012-9349-8.
[24] Pitt HA, Nakeeb A. Chapter 8 - bile secretion and pathophysiology of biliary tract obstruction. In: WRBT-BS of the L, editor. Jarnagin biliary tract and Pancreas, 2-volume set. Sixth Edition. Philadelphia: Elsevier; 2017. 123–132.e1. https://doi.org/10.1016/B978-0-323-34062-5.00008-X.
[25] Beltrán MA, Beltrán AA. Common bile duct pressure in patients with and without cholelithiasis: a case-control study. J Hepatobiliary Pancreat Sci 2021;28:443–449. https://doi.org/10.1002/jhbp.931.
[26] Wiener SM, Hoyt RF, Deleonardis JR, et al. Manometric changes during retrograde biliary infusion in mice. Am J Physiol - Gastrointest Liver Physiol 2000;279:G49–G66. https://doi.org/10.1152/ajpgi.2000.279.1.g49.
[27] Yang J, Lu B. Establishment of a novel rat model of severe acute cholangitis. Iran J Basic Med Sci 2015;18:1124–1129.
[28] Carta L, Wagenseil JE, Knutsen RH, et al. Discrete contributions of elastic fiber components to arterial development and mechanical compliance. Arterioscler Thromb Vasc Biol 2009;29:2083–2089. https://doi.org/10.1161/ATVBAHA.109.193227.
[29] Briones AM, González JM, Somoza B, et al. Role of elastin in spontaneously hypertensive rat small mesenteric artery remodelling. J Physiol 2003;552:185–195. https://doi.org/10.1113/jphysiol.2003.046904.
[30] Hernanz R, Martín Á, Pérez-Girón JV, et al. Pioglitazone treatment increases COX-2-derived prostacyclin production and reduces oxidative stress in hypertensive rats: role in vascular function. Br J Pharmacol 2012;166:1303–1319. https://doi.org/10.1111/j.1476-5381.2012.01825.x.
[31] de Jong IEM, Wells RG. In utero extrahepatic bile duct damage and repair: implications for biliary atresia. Pediatr Dev Pathol 2024;27:291–310. https://doi.org/10.1177/10935266241247479.
[32] Du Y, Khandekar G, Llewellyn J, et al. A bile duct-on-a-chip with organ-level functions. Hepatology 2020;71:1350–1363. https://doi.org/10.1002/hep.30918.
[33] Wang JHC, Thampatty BP, Lin JS, et al. Mechanoregulation of gene expression in fibroblasts. Gene 2007;391:1–15. https://doi.org/10.1016/j.gene.2007.01.014.
[34] Furuya K, Sokabe M, Furuya S. Characteristics of subepithelial fibroblasts as a mechano-sensor in the intestine: cell-shape-dependent ATP release and P2Y1 signaling. J Cel Sci 2005;118:3289–3304. https://doi.org/10.1242/jcs.02453.
[35] Yang Y, Wang J, Zhan Y, et al. The synthetic toxin biliatresone causes biliary atresia in mice. Lab Investig 2020;100:1425–1435. https://doi.org/10.1038/s41374-020-0467-7.
[36] Zhao X, Lorent K, Escobar-Zarate D, et al. Impaired redox and protein homeostasis as risk factors and therapeutic targets in toxin-induced biliary atresia. Gastroenterology 2020;159:1068–1084.e2. https://doi.org/10.1053/j.gastro.2020.05.080.
[37] Tam PKH, Wells RG, Tang CSM, et al. Biliary atresia. Nat Rev Dis Prim 2024;10:47. https://doi.org/10.1038/s41572-024-00533-x.

Keywords:Pressure myography; elastin; mechanobiology; stiffness; bile duct mechanics; collagen.
Received 17 May 2024; received in revised form 28 August 2024; accepted 3 September 2024; Available online 8 September 2024